García Cortijo, S.; Gasulla Mestre, I. (2016). Dispersion-engineered multicore fibers for distributed radiofrequency signal processing. Optics Express. 24(18):20641-20654. doi:10.1364/OE.24.020641.

Dispersion-engineered multicore fibers for distributed radiofrequency signal processing

SERGI GARCÍA* AND IVANA GASULLA

ITEAM Research Institute, Universitat Politècnica de València, Camino de Vera s/n, 46022 Valencia, Spain.
**sergarc3@iteam.upv.es*

Abstract: We report a trench-assisted heterogeneous multicore fiber optimized in terms of higher-order dispersion and crosstalk for radiofrequency true time delay operation. The analysis of the influence of the core refractive index profile on the dispersion slope and effective index reveals a tradeoff between the behavior of the crosstalk against fiber curvatures and the linearity of the propagation group delay. We investigate the optimization of the multicore fiber in the framework of this tradeoff and present a design that features a group delay relative error below 5% for an optical wavelength range up to 100 nm and a crosstalk level below -80 dB for bending radii larger than 103 mm. The performance of the true time delay line is validated in the context of microwave signal filtering and optical beamforming for phased array antennas. This work opens the way towards the development of compact fiber-integrated solutions that enable the implementation of a wide variety of distributed signal processing functionalities that will be key in future fiber-wireless communications networks and systems.

OCIS Codes: (060.2330) Fiber optics communications; (060.2360) Fiber optics links and subsystems; (060.5625) Radio frequency photonics; (350.4010) Microwaves.

References and Links

1. Samsung Electronics Co, "5G Vision", available at http://www.samsung.com/global/business-images/insights/2015/Samsung-5G-Vision-0.pdf, (2015).
2. J. Yao, "Microwave photonics," J. Lightwave Technol. **27**(3), 314-335 (2009).
3. J. Capmany, J. Mora, I. Gasulla, J. Sancho, J. Lloret, and S. Sales, "Microwave photonic signal processing," J. Lightwave Technol., **31**(4), 571-586 (2013).
4. I. Gasulla and J. Capmany, "Microwave photonics applications of multicore fibers," IEEE Photonics J. **4**(3), 877-887 (2012).
5. S. Garcia and I. Gasulla, "Design of heterogeneous multicore fibers as samples true-time delay lines," Opt. Lett. **40**(4), 621-624 (2015).
6. S. Garcia and I. Gasulla, "Crosstalk-optimized multicore fiber true time delay lines," in *Proceedings of IEEE 2015 Int. Topical Meeting on Microwave Photonics* (IEEE, 2015).
7. J. Wang, R. Ashrafi, R. Adams, I. Glesk, I. Gasulla, J. Capmany, and L. R. Chen, "Subwavelength grating enabled on-chip ultra-compact optical true time delay line," Sci. Reports **6**(30235), (2016).
8. M. Koshiba, K. Saitoh, and Y. Kokubun, "Heterogeneous multi-core fibers: proposal and design principle," IEICE Electron. Express **6**(2), 98-103 (2009).
9. K. Saitoh and S. Matsuo, "Multicore fiber technology," J. Lightwave Technol. **34**(1), 55-66 (2016).
10. M. Koshiba, "Design aspects of multicore optical fibers for high-capacity long-haul transmission", *in Proceedings of IEEE 2014 Int. Topical Meeting on Microwave Photonics* (IEEE, 2014), 318-323.
11. T. Hayashi, T. Sasaki, E. Sasaoka, K. Saitoh, and M. Koshiba, "Physical interpretation of intercore crosstalk in multicore fiber: effects of macrobend, structure fluctuation and microbend," Opt. Express **21**(5), 5401-5412 (2013).
12. J. Tu, K. Saitoh, M. Koshiba, K. Takenaga, and S. Matsuo, "Optimized design method for bend-insensitive heterogeneous trench-assisted multi-core fiber with ultra-low crosstalk and high core density," J. Lightwave Technol. **31**(15), 2590-2598 (2013).
13. J. Tu, K. Long, and K. Saitoh, "An efficient core selection method for heterogeneous trench-assisted multi-core fiber," IEEE Photonics Technol. Lett. **28**(7), 810-813 (2016).
14. J. Tu, K. Saitoh, M. Koshiba, K. Takenaga, and S. Matsuo, "Design and analysis of large-effective-area heterogeneous trench-assisted multi-core fiber," Opt. Express **20**(14), 15157-15170 (2012).
15. A. Yariv and P. Yeh, *Photonics. Optical electronics in modern communications*, (Oxford University Press, 2007), Chap. 14.

16. T. Hayashi, T. Taru, O. Shimakawa, T. Sasaki, and E. Sasaoka, "Ultra-low-crosstalk multi-core fiber feasible to ultra-long-haul transmission," in *Proceedings Opt. Fiber Commun. Conf./Nat. Fiber Opt. Commun.* (OFC/NFOEC, 2011).
17. J. Mu, L. Han, Z. Yu, L. Liu, X. Wu, H. Yin, and X. Song, "Study of trench-assisted single mode optical fiber," in *Proceedings of 3rd International Conference on Consumer Electronics, Communications and Networks* (IEEE, 2013).
18. R. J. Mailloux, *Phased Array Antenna Handbook*, (Dedham, MA: Artech House Publishing Co., 2nd ed., 2000).

1. Introduction

Next generation global-scale Information Technology scenarios, such as 5G communications and the Internet of Things, will require new optical technologies to address the current limitations to massive capacity and connectivity, [1]. This involves a full convergence between the optical fiber and the wireless network segments in terms of: (1) radio access distribution between a central office and different remote locations, including Multiple Input Multiple Output antenna connectivity; and (2) broadband microwave photonics (MWP) signal processing [2,3]. In our way to offer a compact and smooth fiber-wireless matching solution, we have proposed the use of heterogeneous multicore fibers (MCFs) as the medium to provide both distribution and processing functionalities "simultaneously", leading to the novel concept of "fiber-distributed signal processing" [4-6]. This approach requires the use of heterogeneous MCFs that are dispersion engineered to operate as group-index-variable optical delay lines offering true time delay line (TTDL) operation for radiofrequency (RF) signals. The TTDL is actually the basis of multiple MWP signal processing applications that will be key in future fiber-wireless communications such as reconfigurable microwave signal filtering and squint-free radio beamsteering in phased array antennas [2,3].

A group-index-variable delay line, as opposed to length-variable TTDLs, implies a variation in the propagation velocity of the optical fiber cores or waveguides involved [7]. In the case of a heterogeneous MCF, we can achieve a constant group delay difference between the TTDL samples, i.e. between adjacent cores, by properly designing the dispersion and refractive index profile of each single core, [5,6]. Moreover, this group delay difference must feature a linearly incremental behavior with the optical wavelength to assure the tunability of the delay line. The optimization of the higher-order dispersion for each individual core will allow to preserve the TTDL linear performance for a broad optical wavelength range. This will guarantee the viability of the envisioned delay line as a promising optical technology to provide both microwave signal processing and radio over fiber distribution within a single optical fiber. Figure 1 illustrates the rationale of a communications application scenario built upon the MCF-based TTDL, covering from fiber distribution over a passive optical network (PON) to multiple MWP signal processing functionalities, such as squint-free radio beamsteering, arbitrary waveform generation and microwave signal filtering.

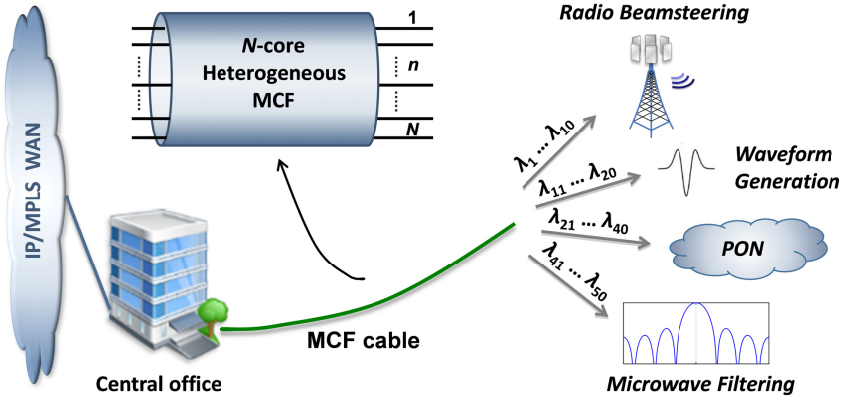

Fig. 1. Application scenario where a single heterogeneous MCF provides both fiber distribution and different signal processing functionalities over different optical bandwidths.

In this paper, we report a trench-assisted heterogeneous MCF optimized in terms of higher-order-dispersion nonlinearities and crosstalk for broadband TTDL operation. For the first time to our knowledge, we analyze the dispersion slope dependence on the refractive index profile parameters of each individual core. We then design a particular optimized MCF where the group delay error due to higher-order-dispersion is minimized and, therefore, the optical wavelength operation range is increased. Finally, the viability of the designed MCF-based TTDL is demonstrated in the context of microwave signal filtering and optical beamforming for phased array antennas.

2. Dispersion and crosstalk optimization

2.1 Differential group delay: Spatial and optical wavelength diversities

The design of a heterogeneous MCF to behave as a group-index-variable delay line implies that each core features an independent group delay with a linear dependence on the optical wavelength λ, as shown in Fig. 2(c). We can expand the group delay per unit length, $\tau_n(\lambda)$, as a third-order Taylor series around an anchor wavelength λ_0 as:

$$\tau_n(\lambda) = \tau_n(\lambda_0) + D_n(\lambda - \lambda_0) + \frac{1}{2} S_n(\lambda - \lambda_0)^2, \tag{1}$$

where D_n is the chromatic dispersion parameter and S_n the dispersion slope of the core n. For proper true time delay operability, we must design the refractive index profile of each core such that, first, D_n increases with the core number in a constantly incremental fashion and, secondly, we ensure a linear behavior of the group delay along the desired wavelength range. As Eq. (1) shows, to reduce the quadratic wavelength-dependent term and thus maintain the linear performance of the TTDL, we must address a rigorous higher-order dispersion analysis and management. This group-index-variable delay line can actually work on two different operation regimes whether we exploit the spatial or the optical wavelength diversities [4,5]. The delay difference between adjacent samples, that is, the basic differential delay, obeys a different law depending on this operation regime and, as consequence, we must address every regime individually for a proper dispersion optimization.

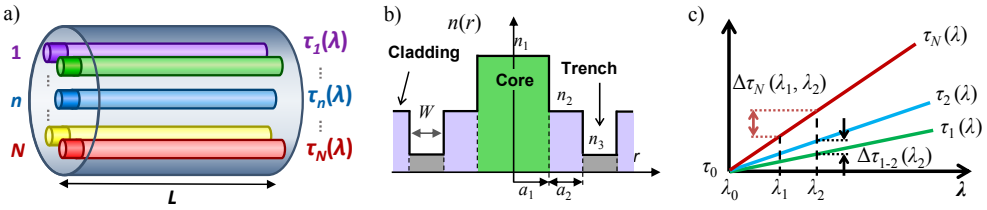

Fig. 2. (a) Heterogeneous N-core MCF. (b) Refractive index profile of a trench-assisted core. (c) Group delay slopes for the N cores showing spatial and optical wavelength diversities.

In the case of spatial diversity, the differential group delay $\Delta\tau_{n,n+1}$ is given by the propagation difference created between each pair of adjacent cores for a particular optical wavelength λ_m:

$$\Delta\tau_{n,n+1}(\lambda_m) = \Delta D(\lambda_m - \lambda_0) + \frac{S_{n+1} - S_n}{2}(\lambda_m - \lambda_0)^2, \tag{2}$$

where $\Delta D = D_{n+1} - D_n$ is the incremental dispersion parameter that is kept constant for every pair of cores. We see from Eq. (2), that the linear wavelength-dependent differential delay is affected by a quadratic term that depends on the difference between the dispersion slopes of the cores involved. We can define the differential group delay relative error induced by this

nonlinear variation as the ratio between the second and the first terms of the right-hand side of Eq. (2), that is:

$$\Delta\tau_{n,n+1}(\lambda_m)\big|_{rel\_err} = \frac{S_{n+1}-S_n}{2\Delta D}(\lambda_m-\lambda_0), \tag{3}$$

which shows that the detrimental nonlinear effect raised by the dispersion slope variability increases with the operation wavelength.

When the delay line operates in the optical wavelength diversity domain, the differential group delay experienced between two contiguous wavelengths (λ_m, λ_{m+1}) in a particular core n is given by:

$$\Delta\tau_n(\lambda_m,\lambda_{m+1}) = D_n\delta\lambda + S_n(\lambda_1-\lambda_0)\delta\lambda + \frac{1}{2}S_n(2m-1)\delta\lambda^2, \tag{4}$$

where $\delta\lambda = \lambda_{m+1} - \lambda_m$ is the separation between the two adjacent optical sources, λ_1 the wavelength of the first optical source and $1 \le m \le M-1$, being M the total number of optical sources. In this case, the undesired variation on $\Delta\tau_n$ is characterized by both the linear ($\delta\lambda$) and the quadratic ($\delta\lambda^2$) dependence on the dispersion slope in Eq. (4), leading to a differential group delay relative error defined as:

$$\Delta\tau_n(\lambda_m,\lambda_{m+1})\big|_{rel\_err} = \frac{S_n\left[(\lambda_1-\lambda_0)+\frac{1}{2}(2m-1)\delta\lambda\right]}{D_n}. \tag{5}$$

As Eq. (5) shows, when we exploit the wavelength diversity, the differential group delay relative error depends on the values of both S_n and D_n of the particular core used. The use of the spatial diversity, instead, causes this error to depend on the variabilities between cores ΔS and ΔD, as shown in Eq. (3).

2.2 Dispersion and crosstalk evaluation

The MCF-based TTDL not only requires optimization in terms of true time delay operability, but also in terms of intercore crosstalk. This implies that, first, both the dispersion parameter and the dispersion slope of each core must fulfil a set of specific rules for TTDL operability [5,6], and, secondly, that we must assure a range of core effective indices as to minimize the intercore crosstalk, [13]. We must, therefore, select the parameters defining the trench-assisted refractive index profile of each core as to satisfy both conditions.

Figure 3 shows the computed dispersion parameter D, dispersion slope S and effective index n_{eff} as a function of the core radius a_1 for three representative sets of design parameters that are defined in Fig. 2(b). Each colored zone corresponds to a particular group of values for the core-to-cladding relative index difference Δ_1, the core-to-trench separation a_2 and the trench width w. The yellow zone is characterized by having high core radii ($4.5 \le a_1 \le 6$ μm) and low core-to-cladding relative index differences ($0.25 \le \Delta_1 \le 0.31\%$), while the rest of the parameters are within the range $3 \le a_2 \le 7$ μm and $4 \le w \le 7$ μm. The orange areas have moderate core radii ($3.4 \le a_1 \le 5$ μm) and core-to-cladding relative index differences ($0.33 \le \Delta_1 \le 0.39\%$), for a combination of $2 \le a_2 \le 6$ μm and $3 \le w \le 6$ μm. Finally, the blue zones own low core radii ($2 \le a_1 \le 3.4$ μm), high core-to-cladding relative index differences ($0.72 \le \Delta_1 \le 0.8\%$), and core-to-trench distances and trench widths, respectively, of $2 \le a_2$ and $w \le 5$ μm. In general, the upper and lower limits of each design variable have been carefully selected as to satisfy, respectively, the single-mode condition and a low level of bend losses, [13,17]. Furthermore, we observe that a value of a_2 above its higher limit will decrease the value of D below the target range for delay line operability. This target range is chosen in a way that the values of D are high enough as to reduce the influence of the nonlinearities raised by S in the wavelength-diversity mode, (see Eq. 5). We must note that quite the

opposite will be found in other applications, such as long-haul high-capacity digital communications, where the target is to reduce the effect of the chromatic dispersion as much as possible.

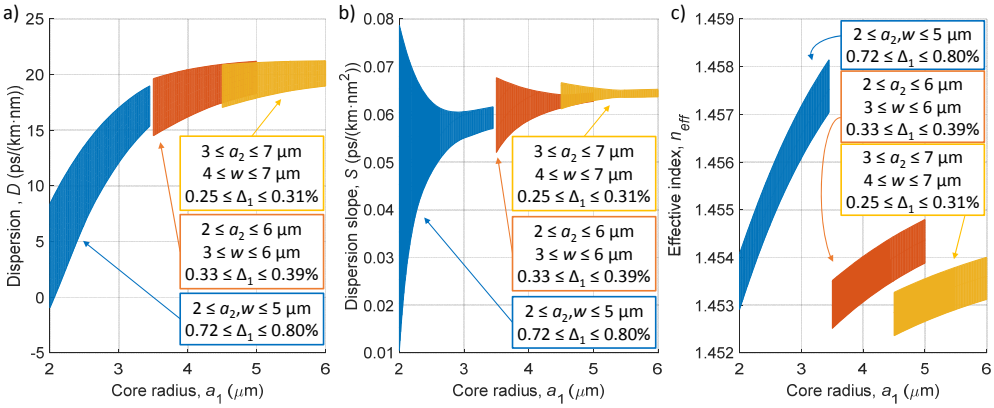

Fig. 3. Comparison between the possible (a) dispersion parameter D, (b) dispersion slope S and (c) effective index n_{eff} values versus the core radius (a_1) for three representative zones (different colors) that are characterized by a particular set of values of the core-to-cladding relative index difference (Δ_1), core-to-trench distance (a_2) and trench width (w).

Since we will consider a 7-core MCF characterized by ΔD = 1 ps/(km·nm), we must assure first a range of dispersion parameter values up to $D_7 - D_1$ = 6 ps/(km·nm) to implement a 7-sample delay line. From Fig. 3(a) we observe that, as long as the core radius increases, the range of dispersion values available decreases, limiting the number of samples that could offer the designed delay line. Secondly, from the previous section, we learned that to reach broadband delay line operability we must: (1) reduce the dispersion slope variability $S_{n+1} - S_n$ between cores as much as possible for spatial-diversity operation (Eq. (3)); and (2) assure a dispersion parameter value D as high as possible for the wavelength-diversity regime (Eq. (5)). From Figs. 3 (a) and (b), we see that increasing the core radius leads to a lower dispersion slope variability and also to higher values of the dispersion parameter D. Thus, we conclude that the optimum zone regarding TTDL operation is the one marked in orange, which allows the required 6 ps/(km·nm) dispersion range with the highest dispersion parameter values and the lowest dispersion slope variability possible.

One of the major challenges found in the design of heterogeneous MCFs is actually the management of the crosstalk dependence on the phase-matching condition between the dissimilar cores when the fiber is bent, [8-12]. To prevent this phase-matching effect, the applied bend curvature radius must be larger than the fiber threshold bending radius, which is defined as the highest radius than can actually induce phase match [10-12]. This threshold bending radius is inversely proportional to the difference between the effective refractive indices of two adjacent cores, [13]. A 7-core MCF with hexagonal disposition requires at least 3 types of cores with similar effective indices to maximize the effective index difference and thus reduce the threshold bending radius. Bend-insensitive MCFs require a minimum effective index difference between adjacent cores of 0.1% for a 35-μm core pitch, [14]. Keeping this in mind, we should choose a design zone that assures a range of effective index differences above 0.2%. In this regard, Fig. 3(c) shows that the areas with low core radii (blue zone) are the optimum ones in terms of intercore crosstalk. However, we must keep in mind that we need to fulfil (to the greatest extent possible) the requirements for both delay line operation and intercore crosstalk. Therefore, we finally choose the orange design area as the candidate to build the proposed dispersion- and crosstalk-engineered MCF.

Once we have identified the range of parameters that enable linear true time delay characteristics with the best crosstalk performance possible, we will carefully evaluate the

influence of the core and trench refractive index profile on the behavior of both the higher-order dispersion and the effective index.

We analyze in first place the behavior of the dispersion slope *S*. Actually, as far as we know, this analysis is the first one carried out for trench-assisted core configurations and provides a useful tool for the design of both homogeneous and heterogeneous MCFs, not only in the context of MWP signal processing, but also for digital communications and sensing applications. Fig. 4(a) shows the dependence of the computed dispersion slope *S* with the core-to-trench distance a_2 for a 4-μm trench width *w* and three significant core radii a_1 (3.4, 4.3 and 5.0 μm plotted in different colors) and core-to-cladding relative index difference Δ_1 (0.33, 0.36 and 0.39% in different line styles). We observe that an increase in a_1 results in a shorter range of variability for *S*, as we have previously deduced from Fig. 3(b), while an increase in Δ_1 has a similar but less significant effect. We find as well that the core-to-trench distance a_2 is the parameter that induces the highest variation on the dispersion slope, provided that a_1 is small enough. Fig. 4(b) illustrates the computed dispersion slope behavior against the core-to-trench distance for different values of the trench width with fixed values of a_1 = 4 μm and Δ_1 = 0.36%. In this case, wider trenches result in a negligible increment on *S* for high values of a_2, which gradually gains relevance as a_2 decreases.

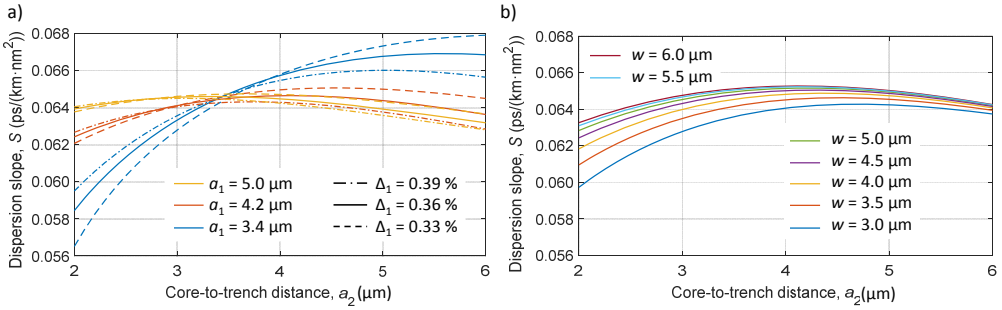

Fig. 4. Dispersion slope dependence on the core-to-trench distance a_2 versus (a) different core radii a_1 (color lines) and core-to-cladding relative index differences Δ_1 (line styles) for a fixed trench width *w* = 4 μm; and (b) different trench widths for a_1 = 4 μm and Δ_1 = 0.36%.

The next step in the optimization technique is the management of the crosstalk and its sensitivity against fiber curvatures. This requires a design of the refractive index profile as to maximize the effective index difference between adjacent cores. Fig. 5(a) shows the dependence of the effective index n_{eff} with the core radius a_1 and the core-to-trench relative index difference Δ_1. We see that increasing a_1 and/or Δ_1 leads to higher effective indices. In this case, we can achieve a variation up to 0.15% by varying both a_1 and Δ_1 (for a fixed a_2 = 4 μm and *w* = 4 μm). Fig. 5(b) illustrates the effective index variation as a function of both a_2 and *w* for a_1 = 4 μm and Δ_1 = 0.36%. We see here that the effective index is not affected by a variation in *w* at all, while it raises as the core-to-trench distance increases. Actually, the separation between the core and the trench affects in a similar trend both the effective index and the dispersion slope in the sense that, as long as this distance is kept in a small range (up to 3 μm), a small change causes the higher variation on the effective index. All in all, only a maximum effective index variation of around 0.02% can be achieved by tuning a_2. As a consequence, we conclude that the core region of the refractive index profile (defined by both a_1 and Δ_1) has the biggest influence on the effective index, as compared to the trench region.

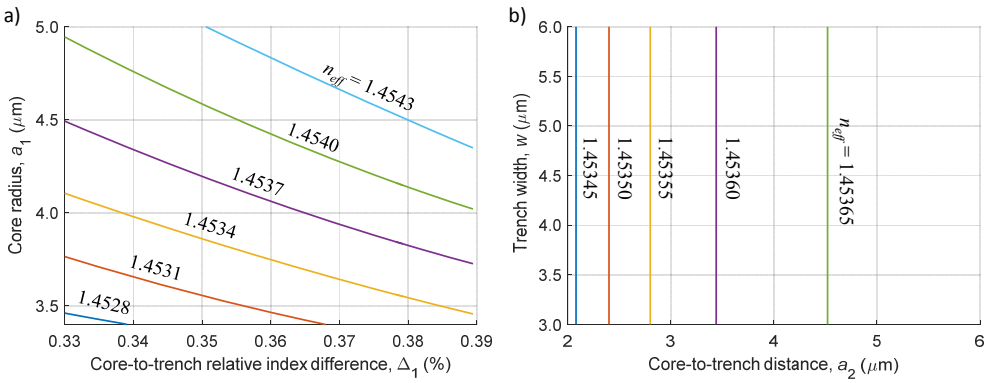

Fig. 5. Effective index dependence on (a) the core radius a_1 versus the core-to-cladding relative index difference Δ_1 for a core-to-trench distance a_2 = 4 µm and trench width w = 4 µm; and (b) the trench width w versus the core-to-trench distance a_2 for a_1 = 4 µm and Δ_1 = 0.36%.

2.3 Design optimization in terms of higher-order dispersion

Once evaluated the influence of the trench-assisted core refractive index profile on both the dispersion slope and the effective index, we developed a particular higher-order-dispersion- and crosstalk- engineered design that ensures a linear group delay in a broad input wavelength range. The designed fiber is composed of seven trench-assisted heterogeneous cores (35-µm core pitch and 125-µm cladding diameter) placed in a hexagonal disposition. By using the *Photon Design* numerical software *Fimmwave*, we obtained a range of D values from 14.75 up to 20.75 ps/(km·nm) with an incremental dispersion ΔD = 1 ps/(km·nm). The fiber satisfies as well the common group index condition at λ_0 = 1550 nm, as reported in [5,6]. Table 1 gathers all the core design variables as well as the computed dispersion slopes, effective indices and effective areas. The cladding-to-trench relative index was fixed to $\Delta_2 \approx$ 1% in all cores.

Table 1. Core design parameters and properties for the dispersion-slope-optimized design

Core n	Core design parameters				Core Properties		
	a_1 (µm)	Δ_1 (%)	a_2 (µm)	w (µm)	S (ps/(km·nm^2))	n_{eff}	A_{eff} (µm^2)
1	3.42	0.3864	5.48	3.02	0.06527	1.453384	64
2	3.60	0.3762	5.03	2.61	0.06434	1.453465	66
3	3.62	0.3690	4.35	3.32	0.06496	1.453386	65
4	4.26	0.3588	4.92	4.67	0.06446	1.453881	75
5	3.49	0.3476	2.81	5.41	0.06431	1.452878	59
6	4.79	0.3435	3.35	3.32	0.06425	1.454041	81
7	4.98	0.3333	2.42	4.05	0.06422	1.453979	82

The design technique was carried out by distributing three groups of cores on the cross-sectional area of the fiber, where each group comprises cores that feature similar effective indices. The groups are formed as follows: (group 1) a central or inner core identified with the lowest effective index; (group 2) three outer cores placed in non-adjacent positions with intermediate values of the effective index and (group 3) three outer cores placed in alternate positions as well featuring the highest effective indices. The core labelled as 5 was chosen as the inner core, having the lowest effective index. To achieve this effective index reduction, its core radius and core-to-trench distance were reduced, while the trench width was highly increased and the core-to-cladding relative index difference was set to an intermediate value.

Group 2 is formed by cores 1, 2 and 3, which feature a low core radius, high core-to-cladding relative index difference and high core-to-trench distance. This leads to a *S* variability below 0.001 ps/(km·nm^2) and an effective index around 1.4534. Cores 4, 6 and 7 constitute the group 3. They are characterized by a higher core radius, lower core-to-cladding relative index difference and lower core-to-trench distance to keep the low S variability along all the cores.

The design of the MCF revealed an important tradeoff between the dispersion slope and the effective index difference between adjacent cores in the sense that maximizing the effective index difference increases the range of variability of the dispersion slope. Fig. 6 shows the computed dispersion slope versus the effective index for the set of design parameters that satisfy the target true time delay line requirements, i.e., common group index and dispersion requirements. Each small circle in the figure corresponds to the effective index and the dispersion slope obtained for particular values of the design variables. The seven different colors are used to distinguish the value of the dispersion parameter *D* that is actually linked to a specific core number. Filled squares represent each of the designed cores, named as C1-C7 respectively for cores 1 to 7. We see here how the magnitude of the dispersion slope is reduced as the effective index decreases, leading to an increment on the dispersion slope variability between the core featuring the lowest effective index (i.e., C5) and the rest. As shown, all the cores of the optimized MCF (i.e., filled squares) have the highest effective index possible, presenting at the same a dispersion slope with the most similar values. On the other hand, we observe that the intercore crosstalk behavior can improve if the limitation on the maximum dispersion slope variability becomes less restrictive. Therefore, we propose to develop a second heterogeneous MCF in which we prioritize the effective index optimization over the dispersion slope optimization, so that we can compare both structures in terms of crosstalk and TTDL operation and choose the proper one for a given application scenario.

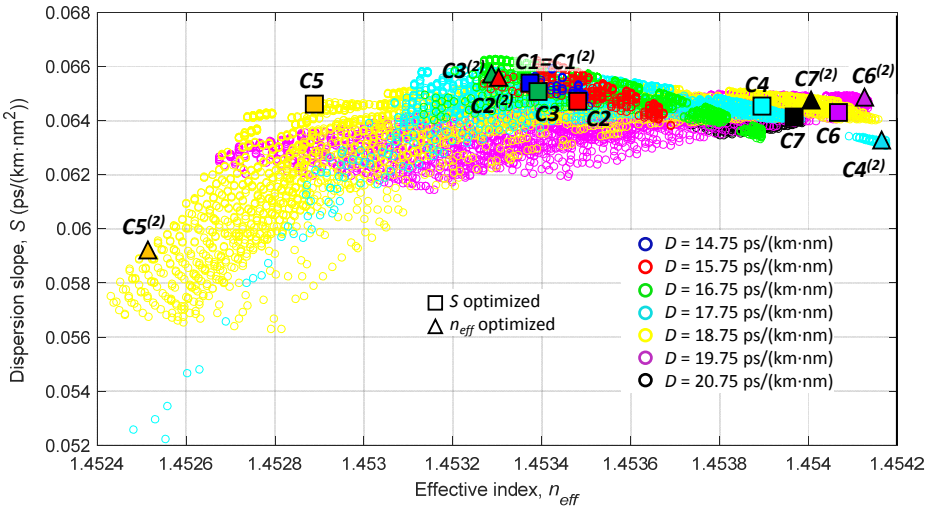

Fig. 6. Relationship between the computed dispersion slopes *S* and effective indices n_{eff} for a group index of 1.4755 and dispersion values *D* ranging from 14.75 up to 20.75 ps/(km·nm), plotted in different colored circles. Filled squares illustrate the *S* and n_{eff} of cores 1-7 for the particular dispersion-slope-optimized MCF, while filled triangles for the effective-index-optimized MCF.

2.4 Design optimization in terms of intercore crosstalk

We present here a new particular design that prioritizes the optimization of the effective index over optimization of the dispersion slope. This MCF share the same TTDL requirements and characteristics, (such as the range of dispersion parameters *D* and the common group index)

as the previous design reported in subsection 2.3. Table 2 gathers the core design parameters and propagation properties. The main difference between both fibers is that the core with the lowest effective index (core 5) is designed as to minimize the value of the effective index rather than to reduce the dispersion slope variability. This way, all the core radius, core-to-cladding relative index difference and core-to-trench distance have been reduced to achieve an effective index close to 1.4525, leading to a maximum dispersion slope variability between adjacent cores at least six times higher. Fig. 5 shows actually the comparison between the effective indices and dispersion slopes of both designs, where the cores of this new design are identified with filled triangles and the superscript (2). This figure is very helpful to illustrate the tradeoff between S and n_{eff} that actually exists in heterogeneous MCFs. On one hand, this tradeoff limits the maximum effective index difference that we can reach if our goal is to reduce the variability in the values of the higher-order dispersion and, on the other hand, it limits the minimum range of dispersion slope values that we can obtain when our goal is to optimize the fiber in terms of crosstalk.

Table 2. Core design parameters and properties for the effective-index-optimized design

Core	Core design parameters				Core Properties		
n	a_1 (μm)	Δ_1 (%)	a_2 (μm)	w (μm)	S (ps/(km·nm^2))	n_{eff}	A_{eff} (μm^2)
1	3.42	0.3864	5.48	3.02	0.06527	1.453384	64
2	3.40	0.3762	4.68	3.66	0.06591	1.453273	63
3	3.50	0.3690	4.22	4.45	0.06593	1.453270	63
4	4.59	0.3588	5.62	2.14	0.06293	1.454129	81
5	3.41	0.3476	2.20	4.09	0.05915	1.452534	56
6	4.89	0.3435	3.50	3.62	0.06451	1.454126	83
7	5.00	0.3333	2.51	5.12	0.06467	1.454012	83

From both Table 1 and Table 2, we see, as expected, that the effective area A_{eff} increases with the core radius. Actually, the effective areas are gathered around two values: 60 μm^2 for groups of cores 1 and 2, and 80 μm^2 for group 3. Since the fiber-wireless scenarios that we consider for the MCF-based distributed signal processing approach will require link lengths usually not greater than 20 km and low levels of optical power, we can discard the existence of nonlinear optical effects, such as the Kerr effect, [15].

3. True time delay operation and crosstalk validation

Once both the higher-order-dispersion-optimized and the crosstalk-optimized fibers are designed, we will evaluate their performance in terms of true time delay line operation and intercore crosstalk robustness against curvatures.

3.1 True time delay line operation

The performance evaluation of both sampled true time delay lines will be focused only on the spatial diversity mode of operation. Since both fibers share identical TTDL properties (such as the dispersion parameter D), they will feature a very similar differential group delay relative error (as given by Eq. (5)) when we work in the wavelength-diversity regime. Therefore, the evaluation of the wavelength diversity regime is not included here.

Figure 7(a) shows the computed group delay for each core as a function of the optical wavelength for both fiber designs. We observe here that the first requirement for TTDL operation is totally fulfilled, that is, all of the cores share a common group index (and thus common group delay) at the anchor wavelength λ_0 = 1550 nm, [4,5]. To a great extent, the second requirement, i.e. linearly incremental group delay slopes, is also achieved in both fibers. Figs. 7(b) and (c) illustrate the differential group delay due to the nonlinear terms of

Eq. (2) as a function of the wavelength, respectively, for the dispersion-slope-optimized and the effective-index-optimized fibers. As a reference, we also include in dashed lines the group delay relative error calculated from Eq. (3). We see how the maximum relative error due to the dispersion slope variability increases up to 15% within a 50-nm range for the effective-index-optimized design, while it is kept below 2.5% for the dispersion-slope-optimized fiber. In general, we checked that a relative error around 5-10% can be considered as the lower limit from which the target response of a typical MWP application (such as signal filtering or radio beamsteering) is excessively damaged. This implies that the wavelength operation range is wider (larger than 100 nm) in the dispersion-optimized-fiber than in effective-index-optimized one (25-35 nm range).

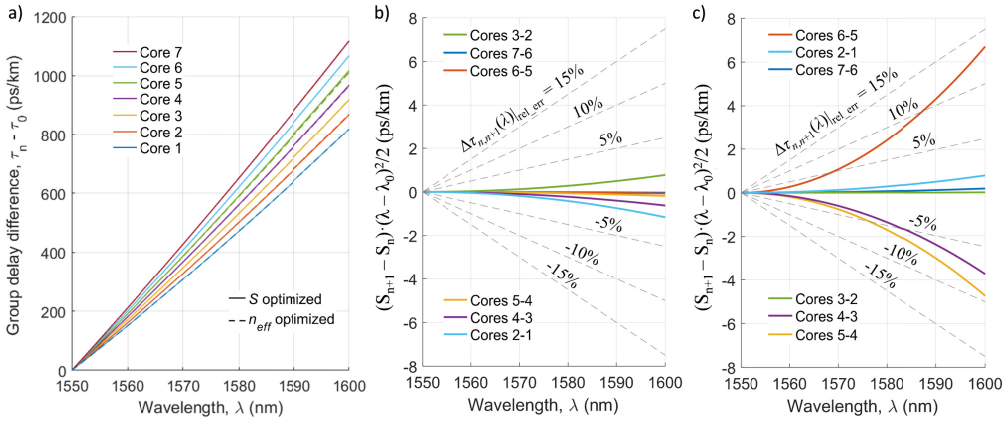

Fig. 7. (a) Computed core group delays versus wavelength for the fiber (dashed lines); Computed differential group delay due to the nonlinear dispersion effect (given by the nonlinear part of Eq. (3)) as a function of the wavelength for (b) the dispersion-slope-optimized fiber and (c) the effective-index-optimized fiber. Dashed lines represent the differential group delay relative error calculated from Eq. (3).

3.2 Crosstalk

One of the major detrimental effects that can degrade the performance of heterogeneous MCFs arises from the crosstalk dependence on the phase-matching condition between adjacent cores when the fiber is bent [10-12]. To overcome this phenomenon, we have optimized our designs by maximizing, as much as possible, the effective index difference Δn_{eff} between adjacent cores as to improve the threshold bending radius R_{pk} [13]. Figs. 8(a) and (b) show the location of the cores on the cross-sectional area of the fiber for the effective-index-optimized and the dispersion-slope-optimized designs, respectively. As described in subsection 2.5, the selected spatial distribution ensures that each of the three groups of similar effective index cores are placed in nonadjacent positions. Fig. 8(c) illustrates the numerical evaluation of the intercore crosstalk dependence on the fiber bending radius in both designs for the pair of cores bringing the worst-case scenario. As shown, the fiber optimized in terms of effective index presents a threshold bending radius R_{pk} close to 69 mm that corresponds to $\Delta n_{eff} \approx 0.074\%$. On the other hand, in the case of the design optimized in terms of higher-order dispersion, the threshold bending radius is shifted to around 103 mm as the effective index difference is reduced down to a 0.050%. In addition, we see that the worst-case crosstalk above the phase-matching region is kept below -80 dB in both designs, which stays in the order of the -70 dB reported for trench-assisted 7-core MCFs [10,16]. When the fibers are bent right at their threshold bending radii, the simulation results show that both designs are very robust against fiber curvature losses as well, reaching a worst-case bend loss below 0.1 dB/km.

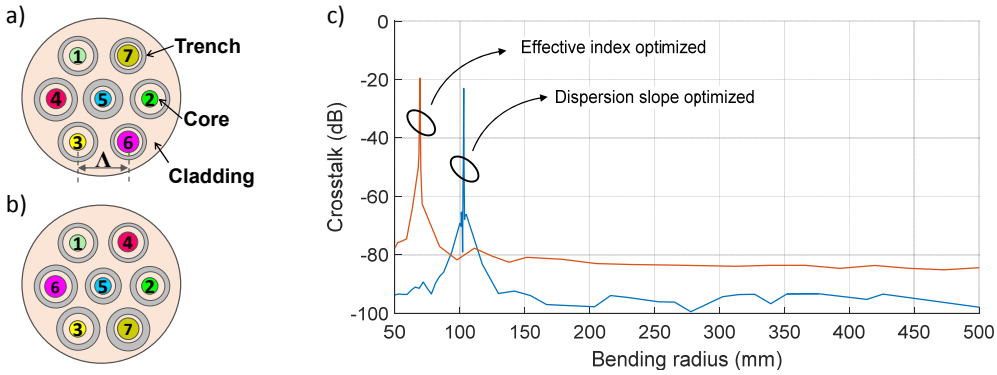

Fig. 8. Cross-sectional fiber view for (a) the effective-index-optimized and (b) the dispersion-slope-optimized designs; (c) Computed crosstalk as a function of the bending radius for the effective-index (solid red) and dispersion-slope-optimized designs (dashed blue).

4. Application to Microwave Photonics distributed signal processing

The developed MCF-based delay lines will serve as a compact and energy efficient solution to implement a variety of MWP signal processing functionalities that will be especially demanded in fiber-wireless communications networks and subsystems. As a proof of concept, we evaluate here their performance as distributed signal processing elements when they are applied to two particularly demanded Microwave Photonics functionalities: tunable microwave signal filtering and optical beamforming for phased array antennas, [2,3]. We will show the importance of properly engineering the higher-order dispersion of the heterogeneous MCF in terms of broadband TTDL operation. We will compare the designs described in section 3 to the ideal responses given by the linear parts of Eqs. (2) and (4) when applying, respectively, the space-diversity or the wavelength-diversity operation regimes. The block diagrams describing how to implement both the filter and the beamforming network from the MCF-based TTDL can be found in [4].

4.1 Microwave signal filtering

A frequency filtering effect over RF signals results from combining and collectively photodetecting (with a single receiver) the delayed signal samples coming from the TTDL output. This incoherent Finite Impulse Response (FIR) filter is then characterized by a transfer function $H(f)$ that is given by, [3]:

$$H(f) = \sum_{n=0}^{N-1} a_n e^{-jn2\pi f \Delta\tau}, \tag{6}$$

where a_n is the weight (amplitude and phase) corresponding to the n^{th} sample and f the RF frequency. The frequency period or Free Spectral Range (FSR) of the microwave filter is given by $FSR = 1/\Delta\tau$, where $\Delta\tau$ is the basic differential delay of the TTDL as defined in section 2.

We evaluate the performance of a TTDL implemented with a 10-km MCF comparing both space and wavelength modes of operation. Figs. 8(a)-(d) illustrate de computed transfer function H of the microwave filter as a function of the RF frequency when the TTDL operates in wavelength diversity. We compare here the response of the filters implemented with the designed TTDLs (blue-solid line) to the ideal response (red-dashed line) obtained by setting S to zero in the basic differential delay given by Eq. (4). As commented before, we obtain the same performance in both dispersion- and crosstalk-optimized fibers when we exploit diversity in optical wavelength. Fig. 9(a) correspond to the case when we use an array of M = 5 lasers from λ = 1550 up to 1554 nm with a 1-nm separation. We see a perfect match between the responses from the ideal and the designed delay elements. If we increase the

wavelength range up to 1590-1594 nm, we observe a considerable mismatch between both responses, as shown in Fig. 9(b). This is caused by the linear $\delta\lambda$-dependence of S in Eq. (4) (second term in right-hand side). However, this linear displacement does not distort the filter shape, so we could compensate a priori this effect by taking into account this wavelength displacement when designing the TTDL. Actually, we can re-tune the response by properly managing the operation wavelengths of the lasers, as shown in Fig. 9(c) when the separation between the input wavelengths is reduced down to 0.89. We can as well compensate that effect by increasing the number of lasers, as shown Fig. 9(d) for $M = 10$. Note that the optical wavelength shift $\delta\lambda$' that compensates this displacement can be easily obtained from Eq. (4) as:

$$\delta\lambda' = \frac{D_n}{D_n + S_n\left(\lambda_1 - \lambda_0\right)}\delta\lambda\,. \tag{7}$$

Figs. 9(e)-(h) represent the computed transfer function H of the microwave filter working in spatial diversity when we compare: (1) the MCF optimized in terms of higher-order dispersion (blue solid lines); (2) the MCF optimized in terms of effective index (green solid lines) and (3) the ideal response (red dashed lines). The 10-km MCF length results in a Free Spectral Range of (e) 10 GHz for an operation wavelength of $\lambda = 1560$ nm, (f) 4 GHz for an operation wavelength of $\lambda = 1575$ nm, (g) 2 GHz for $\lambda = 1600$ nm and (h) 1 GHz for $\lambda = 1650$ nm. As shown, the dispersion-slope-optimized fiber overcomes the limitations induced by the nonlinear effects even for a wavelength range up to 100 nm, while the filter response for the-effective index-optimized fiber is highly degraded for operation wavelengths above 1575 nm.

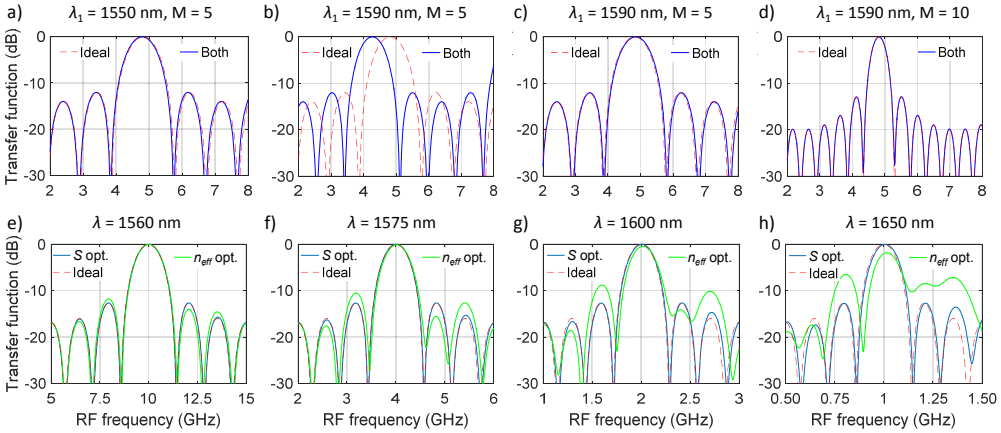

Fig. 9. Comparison of the computed wavelength-diversity transfer function H as a function of the RF frequency for both designs (blue solid line) and the ideal filter (red dashed line) for a 10-km fiber: (a)-(b) set of 5 lasers with a 1-nm separation at an initial wavelength λ_1 of (a) 1550 nm and (b) 1590 nm; (c)-(d) 0.89-nm wavelength separation and $\lambda_1 = 1590$ nm for (c) 5 lasers and (d) 10 lasers. Comparison of the computed spatial-diversity H between the dispersion-optimized (blue solid line), the effective-index-optimized (green solid line) and the ideal filters (red dashed line) for a 10-km fiber at an operation wavelength of (e) 1560 nm, (f) 1575 nm, (g) 1600 nm and (h) 1650 nm.

4.2 Optical beamforming for phased array antennas

Optical beamforming networks are implemented using a similar configuration as in microwave signal filtering, with the particularity that each delayed sample is individually photodetected by an independent receiver and, then, feeds one of the radiating elements that conformed the phased array antenna, [2]. In the case of 1D architectures, the normalized angular far-field pattern of the radiated electric field, or array factor $AF(\theta)$, is given by [18]

$$AF(\theta) = \sum_{n=0}^{N-1} a_n e^{-j2\pi n\nu(\Delta\tau - d_x \sin(\theta)/c)}, \quad (8)$$

where θ is the far field angular coordinate, ν is the optical frequency ($\nu = c/\lambda_0$) and d_x is the spacing between adjacent radiating elements. From Eq. (8), the direction θ_0 of maximum radiated energy can be adjusted by tuning the basic differential delay since $\Delta\tau = d_x \sin(\theta_0)/c$.

We will evaluate the influence of the nonlinearities arisen from both MCFs when they are applied as the TTDL implementing the optical beamforming network for a phased array antenna characterized by d_x = 3 cm, a 5-GHz RF frequency signal and a link length of 10 km. As we have pointed out in the previous microwave filtering analysis, when we operate in wavelength diversity, the nonlinearities arisen in the basic differential delay (term proportional to $\delta\lambda$ in the second term of the right-hand side of Eq. (4)) can be further compensated. Then, for simplicity, our evaluation here focuses only on the use of the spatial diversity. We compare again the dispersion-optimized MCF (blue solid lines), the effective-index-optimized fiber (green solid lines) and the ideal response (red dashed lines). Fig. 10(a) shows the computed array factor as a function of the beam pointing angle (in degrees) in both polar coordinates (left) and decibels (right) at an operation wavelength of λ_m = 1570 nm. We see that, for a 20-nm wavelength range (anchor wavelength λ_0 = 1550 nm), the array factor offered by the effective-index-optimized MCF is slightly mismatched from the ideal one, while the one given by the dispersion-slope-optimized fiber matches it perfectly. If the operation wavelength is increased up to 1600 nm, Fig. 10(b) shows that the array factor is highly degraded when we use the effective-index-optimized fiber, but stays practically unaltered when we resort to the dispersion-slope-optimized fiber instead.

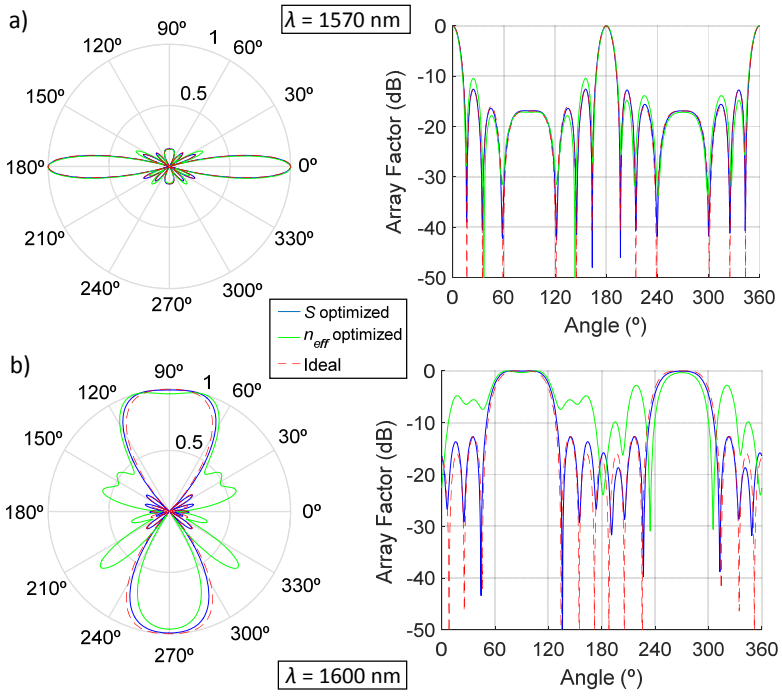

Fig. 10. Comparison between the computed array factor (AF) as a function of the beam pointing angle (in degrees) for the dispersion-slope-optimized MCF (blue solid line), the effective-index-optimized design (green solid line) and the ideal delay line for a 10-km fiber with a $\lambda_{RF}/2$-separation between antennas for a RF frequency of 5 GHz at an operation wavelength of (a) 1570 nm and (b) 1600 nm. Left: in polar coordinates; Right: in decibels.

5. Funding and Acknowledgments

Spanish MINECO TEC2015-62520-ERC Project; Spanish MINECO TEC2014-60378-C2-1-R MEMES Project; Spanish MINECO BES-2015-073359 fellowship for Sergi García; Spanish MINECO Ramón y Cajal Program (RYC-2014-16247) for Ivana Gasulla.

6. Conclusions

We have presented a trench-assisted heterogeneous multicore fiber optimized in terms of higher-order dispersion that is designed to operate as a broadband tunable delay line for radiofrequency signals. For the first time to our knowledge, we have analyzed the influence of the core and trench refractive index profiles on the dispersion slope of a multicore fiber. This allows us to optimize the performance of the multicore fiber in terms of the propagation nonlinearities that affect the group delay of each one of the cores. In general, the optimization provides a useful tool for the design of any type of multicore fiber for a variety of applications, including long-haul high-capacity broadband communications or chromatic dispersion compensation techniques. In the particular application scenario of microwave signal processing for fiber-wireless networks, this optimization is essential for the implementation of sampled true time delay lines that can operate in a broad optical wavelength range, giving support to different functionalities in the same single optical fiber. The investigation of both the dispersion slope and the effective index revealed an important tradeoff between minimizing the sensitivity of the intercore crosstalk against fiber curvatures and the nonlinearities in terms of the propagation group delay. We have designed and compared a dispersion-slope-optimized design and an effective-index-optimized design in order to demonstrate the importance of a proper management of the dispersion slope of the cores. The MCF optimized in terms of higher-order dispersion ensures a delay relative error below 5% for an optical wavelength range up to 100 nm and a crosstalk level below -80 dB for bending radii larger than 103 mm. We demonstrated the viability of this optical fiber as linear true time delay line when it is applied to microwave signal filtering and optical beamforming in phased array antennas.

This work opens the way towards the development of distributed signal processing for microwave and millimeter-wave signals in a single optical fiber where a variety of functionalities can be implemented exploiting different optical wavelength bands. Future fiber-wireless access networks will benefit the proposed multicore fiber approach in terms of: (1) compactness as compared to a set of parallel singlecore singlemode fibers, (2) performance stability against mechanical or environmental conditions and (3) operation versatility offered by the simultaneous use of the spatial- or wavelength-diversity domains.

.